Continuous Growth of Droplet Size Variance due to Condensation in Turbulent Clouds

Gaetano Sardina,[1,*] Francesco Picano,[2,3] Luca Brandt,[2] and Rodrigo Caballero[1]
[1]Department of Meteorology and SeRC, Stockholm University, SE-106 91 Stockholm, Sweden
[2]Linné FLOW Centre and SeRC, KTH Mechanics, SE-100 44 Stockholm, Sweden
[3]Department of Industrial Engineering, University of Padova, 35131 Padova, Italy
(Received 15 December 2014; revised manuscript received 21 May 2015; published 29 October 2015)

We use a stochastic model and direct numerical simulation to study the impact of turbulence on cloud droplet growth by condensation. We show that the variance of the droplet size distribution increases in time as $t^{1/2}$, with growth rate proportional to the large-to-small turbulent scale separation and to the turbulence integral scales but independent of the mean turbulent dissipation. Direct numerical simulations confirm this result and produce realistically broad droplet size spectra over time intervals of 20 min, comparable with the time of rain formation.

DOI: 10.1103/PhysRevLett.115.184501 PACS numbers: 47.55.db, 47.27.Gs, 47.55.-t, 92.60.Nv

Many multiscale processes—including nutrient foraging of plankton, gas or dust accretion disks in astrophysics and spray evaporation and combustion in engines [1–4]—involve the interaction between small particles and tracers transported in a turbulent flow. Here we focus on the case of droplet condensation in turbulent warm (i.e. ice-free) clouds. Clouds are a leading source of uncertainty in climate modeling [5] due to the difficulty of accurately parametrizing the macroscale effects of microscale physical processes, such as the effect of droplet size distribution on precipitation rates and cloud albedos.

The role of turbulence in cloud microphysics presents a range of open questions [6–8], particularly as a possible solution for the "bottleneck" problem of rain formation. All cloud droplet populations evolve through a sequence of steps: (1) nucleation or activation of cloud condensation nuclei, (2) droplet growth by condensation, and (3) growth to raindrop size by collision and coalescence. The passage from (2) to (3) presents a bottleneck because collisional growth is only triggered when the droplet population acquires a sufficiently broad size distribution, but condensational growth is inversely proportional to droplet radius which intrinsically tends to narrow the size distribution. Nonetheless, warm clouds are routinely observed to precipitate within $\sim$20 min of formation. Understanding the mechanisms that break the condensational bottleneck is a longstanding and still unresolved problem in atmospheric physics.

Turbulence has often been invoked as a key process in this context since it can enhance collision rates via inertial clustering [9,10] and the so called "sling effect" [11]. Turbulence also induces fluctuations in the supersaturation field that can potentially broaden droplet spectra in the condensational stage [8]. Early studies using analytical models [12,13] and direct numerical simulations (DNS) [14] generally showed too little broadening as compared with observations [15]. Later work attempting to simulate large-scale turbulence in an $O(100\ \mathrm{m})$ cloud [16–18] showed a dramatic broadening of the droplet size spectrum but only with *ad hoc* assumptions about the small-scale supersaturation fluctuations. Lanotte *et al.* [19] modeled both small- and large-scale effects on the droplet size distribution with simulations of a cloud of 70 cm and pointed out the importance of the Taylor Reynolds number, Re_λ, the nondimensional parameter measuring the large- to small-scale separation in homogeneous isotropic turbulence. In particular, they suggested that droplet spectral broadening should scale with $\mathrm{Re}\lambda$.

A question that has not been addressed so far is the long-term fate of the droplet spectrum: does it reach a steady state, or does it continue to evolve? The large range of scales involved makes DNS very computationally demanding, and all existing simulations consider time spans between a few seconds and 2 min, well below the observed rain formation time scale.

Here, we approach this question by first deriving an analytical expression for the standard deviation of the droplet radius squared (droplet surface area) in terms of the thermodynamics and turbulence characteristics, modeling the fluctuations as stochastic processes. We demonstrate that the droplet size distribution increases monotonically with time as $t^{1/2}$. We validate this analytical result by extending previous numerical results with DNS and large eddy simulations (LES) to time scales comparable with those of rain formation, about 20 min. Our results imply that every warm cloud would precipitate if given enough time. The broadening rate is determined by the large scale turbulent motions and by the positive correlation between droplet surface area and local supersaturation.

Our physical model is analogous to that in [19]; a detailed description can be found in the Supplemental Material [20]. We assume homogeneous isotropic turbulence obeying the incompressible Navier-Stokes equations

$$\frac{\partial \mathbf{u}}{\partial t} + \mathbf{u}\cdot\nabla\mathbf{u} = -\frac{\nabla p}{\rho} + \nu\nabla^2\mathbf{u} + \mathbf{f}, \tag{1}$$

where $\mathbf{u}$ is the divergence-free fluid velocity, p the pressure, ρ the air density, $\mathbf{f}$ an external forcing to maintain a statistically stationary state, and ν the kinematic viscosity. This approximation is valid for clouds smaller than $L \approx 100$ m, which allow spatial inhomogeneity and large-scale variations of the thermodynamic parameters to be safely neglected. The supersaturation field s is transported by the fluid according to

$$\frac{\partial s}{\partial t} + \mathbf{u}\cdot\nabla s = \kappa\nabla^2 s + A_1 w - \frac{s}{\tau_s}, \tag{2}$$

a generalization of the Twomey model [27]. The diffusivity of the water vapor in air is denoted by κ, w is the velocity component in the gravity direction, and $A_1 w$ is a source or sink term of supersaturation resulting from the variation in temperature and pressure with height. The supersaturation relaxation time τ_s depends on droplet concentration and dimensions [28], $\tau_s^{-1} = 4\pi\rho_w A_2 A_3 \sum R_i/V$ where R_i are the radii of the droplets in the volume V, ρ_w the water density, and A_1, A_2, and A_3 thermodynamic coefficients [19]. The droplets are assumed to behave as rigid spheres smaller than the Kolmogorov turbulent scale, at low mass fraction to neglect feedback on the flow. The only forces governing the droplet motion are gravity and the Stokes drag (nucleation and activation are not considered):

$$\frac{d\mathbf{v_d}}{dt} = \frac{\mathbf{u}(\mathbf{x_d}, t) - \mathbf{v_d}}{\tau_d} - g\mathbf{e_z}, \qquad \frac{d\mathbf{x_d}}{dt} = \mathbf{v_d} \tag{3}$$

with $\mathbf{x_d}$ and $\mathbf{v_d}$ the droplet position and velocity, $\mathbf{u}(\mathbf{x_d}, t)$ the fluid velocity at droplet position, $\tau_d = 2\rho_w R_i^2/(9\rho\nu)$ the droplet relaxation time, and g the gravitational acceleration. The supersaturation at the droplet position, $s(\mathbf{x_d}, t)$, determines the droplet evolution via

$$\frac{dR_i^2}{dt} = 2A_3 s(\mathbf{x_d}, t). \tag{4}$$

An exact equation for the average of the droplet radius fluctuations is obtained from (4),

$$\frac{d\langle (R_i^{2'})^2\rangle}{dt} = \frac{d\sigma_{R^2}^2}{dt} = 4A_3\langle s' R^{2'}\rangle \tag{5}$$

showing that $\langle (R_i^{2'})^2\rangle$ increases linearly with time only if the correlation $\langle s' R^{2'}\rangle$ reaches a nonzero statistical steady state.

To quantitatively estimate the droplet growth, we adopt a 1D stochastic model for the velocity fluctuations w_i and the supersaturation field s_i' of the ith droplet. Such an approach implicitly assumes that the small-scale turbulent motions have a negligible influence on the macroscopic observables. This assumption is motivated by previous results revealing the broadening of the droplet size distribution with Re_λ [19] and fully justified *a posteriori* by the numerical simulations presented below.

Homogeneous isotropic turbulence and supersaturation are modeled with two Langevin equations [29]:

$$w_i'(t+dt) = w_i'(t) - \frac{w_i'(t)}{T_0}dt + v_{\mathrm{rms}}\sqrt{2\frac{dt}{T_0}}\xi_i(t), \tag{6}$$

where v_{rms} is the root mean square of the turbulent velocity fluctuations, $\xi(t)$ is a zeromean Gaussian white noise, nondimensionalized in order to be δ correlated in time and T_0 the turbulence integral time scale, and

$$\begin{aligned} s_i'(t+dt) = s_i'(t) &- \frac{s_i'}{T_0}dt + A_1 w_i' dt - \frac{s_i'}{\langle\tau_s\rangle}dt \\ &+ \sqrt{(1-C_{ws}^2)\langle s'^2\rangle\frac{2dt}{T_0}}\eta_i(t) \\ &+ C_{ws}\sqrt{\langle s'^2\rangle\frac{2dt}{T_0}}\xi_i(t) \end{aligned} \tag{7}$$

for the supersaturation with forcing from the velocity field. Here $C_{ws} = \langle w's'\rangle/(v_{\mathrm{rms}}\sqrt{\langle s'^2\rangle})$ is the normalized velocity-supersaturation correlation, and $\langle\tau_s\rangle$ is the supersaturation relaxation time based on the mean droplet radius and $\eta(t)$ zero-mean Gaussian white noise, δ correlated in time. Equation (7) represents a stochastic version of the Twomey model. The mean updraft is zero as the mean supersaturation (the mean droplet radius does not change); entrainment effects [30], collisions, and inhomogeneities are also not considered to analyze the conservative case when the droplet spectral broadening is only induced by supersaturation fluctuations.

From (4), (6), and (7), assuming $\langle\tau_s\rangle \ll T_0$ as in real clouds, the fluctuation correlations become

$$\frac{d\langle s' R^{2'}\rangle}{dt} = A_1\langle w' R^{2'}\rangle + 2A_3\langle s'^2\rangle - \frac{\langle s' R^{2'}\rangle}{\langle\tau_s\rangle}, \tag{8}$$

$$\frac{d\langle w' R^{2'}\rangle}{dt} = 2A_3\langle w's'\rangle - \frac{\langle w' R^{2'}\rangle}{T_0}, \tag{9}$$

$$\frac{d\langle s'^2\rangle}{dt} = 2A_1\langle w's'\rangle - 2\frac{\langle s'^2\rangle}{\langle\tau_s\rangle}, \tag{10}$$

$$\frac{d\langle w's'\rangle}{dt} = A_1 v_{\mathrm{rms}}^2 - \frac{\langle w's'\rangle}{\langle\tau_s\rangle}. \tag{11}$$

Assuming statistically quasisteady state conditions ($d\langle\rangle/dt = 0$) we find that $\langle s'^2\rangle_{qs} = A_1^2 v_{\mathrm{rms}}^2\langle\tau_s\rangle^2$ and

$$\langle s' R^{2'} \rangle_{qs} = 2A_3 A_1^2 v_{\rm rms}^2 \langle \tau_s \rangle^2 T_0 = 2A_3 \langle s'^2 \rangle_{qs} T_0 \qquad (12)$$

which give, using (5),

$$\sigma_{R^2} = \sqrt{8} A_3 A_1 v_{\rm rms} \langle \tau_s \rangle (T_0 t)^{1/2} = \sqrt{8 \langle s'^2 \rangle_{qs}} A_3 (T_0 t)^{1/2}. \qquad (13)$$

The model shows that the variance of the droplet distribution increases monotonically in a turbulent flow even though the supersaturation fluctuations reach a statistical steady state s_{qs}. The correlation $\langle s' R^{2'} \rangle_{qs}$, which is directly responsible for the radius growth rate, is proportional to the level of fluctuations of the supersaturation field and to the integral scale of the turbulence; see (12). Expression (13) can be formulated in terms of Kolmogorov scales since $v_{\rm rms} \simeq {\rm Re}_\lambda^{1/2} v_\eta$ and $T_0 \simeq 0.06 {\rm Re}_\lambda \tau_\eta$ [29]:

$$\sigma_{R^2} \simeq 0.7 A_3 A_1 \nu^{1/2} \langle \tau_s \rangle {\rm Re}_\lambda t^{1/2}. \qquad (14)$$

Note that for $t = T_0$ (short compared with rain formation time) the lower limit proposed in [19] is recovered, $\sigma_{R^2} \simeq {\rm Re}_\lambda^{3/2}$. From (14) we note that σ_{R^2} at a fixed time depends only on the scale separation represented by ${\rm Re}_\lambda$ and not on the value of the mean dissipation inside the clouds. This implies that clouds with different dissipation rate and same Reynolds number have an identical behavior in terms of droplet growth by condensation. The droplet or turbulence condensation dynamics does not depend on the turbulent small scales: the correlation between the supersaturation field and the droplet surface area, governing the distribution broadening, is determined by the large flow scales. This result is in contrast with the belief that the variance of the droplet distribution should not grow indefinitely as turbulence tends to decorrelate the particle size from the local saturation field [8].

To test our predictions, we run simulations by gradually increasing the size of the computational clouds from a few centimeters to 100 m. The governing equations (1)–(4) are solved with a classical pseudospectral code for the fluid phase coupled with a Lagrangian algorithm for the droplets [31]. All cases share the same turbulent kinetic energy dissipation $\varepsilon = 10^{-3}$ m^2 s^{-3}, a value typically measured in stratocumuli. This corresponds to the same small-scale dynamics, with Kolmogorov scale $\eta = (\nu^3/\varepsilon)^{1/4} \approx 1$ mm, Kolmogorov time $\tau_\eta = (\nu/\varepsilon)^{1/2} \approx 0.1$ s, and velocity $v_\eta = \eta/\tau_\eta \approx 1$ cm/s. We examine droplets with two different initial radii, 13 μm and 5 μm, denoted as case 1 and 2, with supersaturation relaxation time $\tau_s = 2.5$ and 7 s, and same concentration (130 droplets per cm^3). The reference temperature and pressure are $\theta_0 = 283$ K and $P = 10^5$ Pa, with $A_1 = 5 \times 10^{-4}$ m^{-1}, $A_2 = 350$ m^3/kg, and $A_3 = 50$ μm^2/s. The simulation parameters are reported in Table I. Note that simulation DNS E1, carrying order 10^9 droplets, is to the best of our knowledge the largest direct numerical simulation of a warm cloud ever performed.

TABLE I. Parameters of the simulations. The resolution N, the cloud size $L_{\rm box}$, the root mean square of the turbulent velocity fluctuations $v_{\rm rms}$, and $T_L = L_{\rm box}/v_{\rm rms}$ an approximation of the large turbulent scales. T_0 indicates the integral time $T_0 = (\pi/2v_{\rm rms}^3) \int [E(k)/k] dk$ with k the wave number and $E(k)$ the turbulent kinetic energy spectra [29]. The total number of droplets is indicated by N_d.

Label	N^3	$L_{\rm box}$ [m]	$v_{\rm rms}$ [m/s]	T_L [s]	T_0 [s]	${\rm Re}_\lambda$	N_d
DNS $A1/2$	64^3	0.08	0.035	2.3	0.64	45	6×10^4
DNS $B1/2$	128^3	0.2	0.05	4	0.95	95	9.8×10^5
DNS $C1/2$	256^3	0.4	0.066	6	1.5	150	9×10^6
DNS D1	1024^3	1.5	0.11	14	3	390	4.4×10^8
DNS E1	2048^3	3	0.12	30	4	600	$3. \times 10^9$
LES F1	512^3	100	0.7	142	33	5000	1.3×10^{14}

The time evolution of $\sigma_{R^2} = \sqrt{\langle (R^{2'})^2 \rangle}$ is shown in Fig. 1 for all cases investigated. The data confirm the predictions from (13), i.e. that $\sigma_{R^2} \propto t^{1/2}$.

The correlation $\langle s' R^{2'} \rangle$ is displayed in the inset of Fig. 1 (thin solid line). In all cases, $\langle s' R^{2'} \rangle$ reaches a statistical steady state, fluctuating around the value determining the growth of σ_{R^2}. The turbulence creates a positive correlation between supersaturation and droplet surface area fluctuations that increases as the turbulent scale separation—i.e. the cloud size—increases. The agreement between the model and the numerical data is remarkable for the largest domain sizes where scale separation is significant and

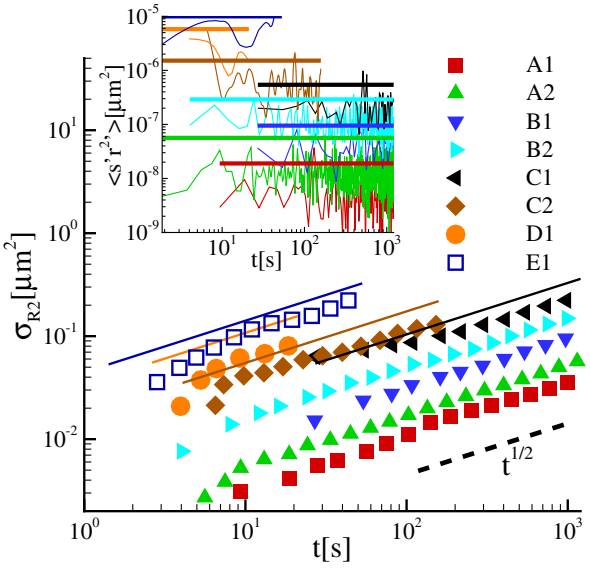

FIG. 1 (color online). Root mean square of the square droplet radius fluctuations σ_{R^2} versus time from simulations (symbols) and the prediction of the stochastic model (13) (lines). Inset: correlation $\langle s' R^{2'} \rangle$ from simulations (thin lines) and from Eq. (12) (thick lines).

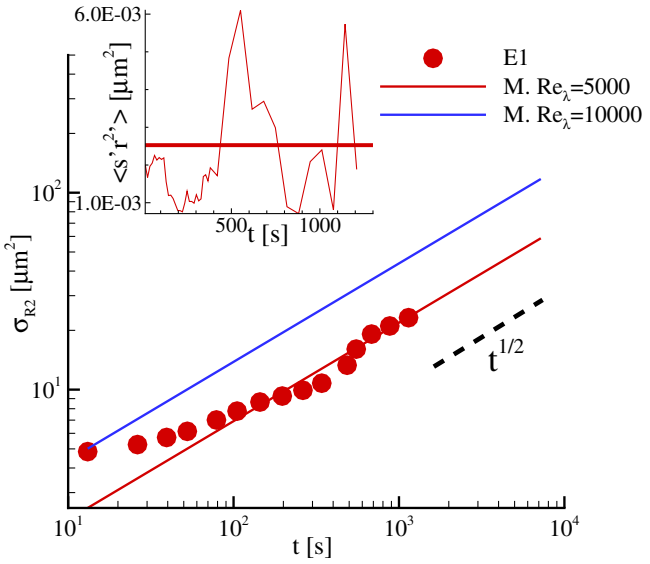

FIG. 2 (color online). Root main square of the square droplet radius fluctuations σ_{R^2} versus time for the LES simulations (symbols) and the model (13) (lines). Inset: correlation $\langle s'R^{2'}\rangle$ from the LES (thin line) and the model (12) [denoted by "M." in the legend (thick lines)].

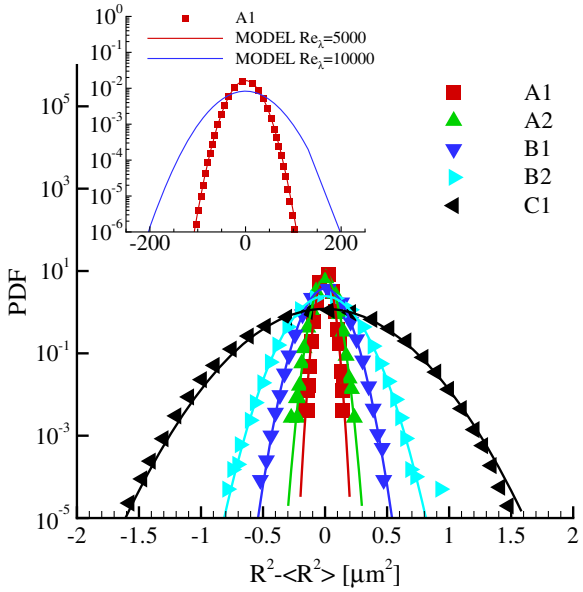

FIG. 3 (color online). Probability density functions (PDFs) of the square radius fluctuations after a simulation time corresponding to about 20 min. (symbols). The lines represent Gaussian distributions with the same variance. The inset reports data from the LES of a large cloud.

viscous effects can be neglected. For small Re_λ, viscous effects are important and the stochastic inviscid model overestimates the correct behavior. For a detailed comparison between DNS and stochastic model, see the Supplemental Material [20].

To test the model for a larger cloud size, we perform a large eddy simulation (LES F1) of a cloud of about 100 m. LES can be seen as a good model for our problem since it fully resolves the larger flow scale, those relevant to droplet condensation or evaporation, as shown above. For numerical details see the Supplemental Material [20]. The Taylor Reynolds number is 5000. The time evolutions of σ_{R^2} and of $\langle s'R^{2'}\rangle$ are depicted in Fig. 2 together with the analytical predictions from (12) and (13). The agreement between the two fully validates our model.

To motivate the use of the variance $\sigma^2_{R^2}$ to define the droplet size distribution, we show in Fig. 3 that its probability distribution is Gaussian, in agreement with measurements in real stratocumuli [32]. The data in the figure refer to the final simulation time (about 20 min) and are compared to Gaussian distributions of equal variance; note that error bars are about the same size as the plotting symbols and not visible in the plot. The size distribution from the LES of the large cloud (see inset) reveals that the Gaussian can be fitted just using the value of σ_{R^2} from the stochastic model also at this higher Reynolds number.

In summary, we have derived an analytical expression for the role of turbulence on the dynamics of droplet condensation and validated it against large-scale numerical simulations. We show that the standard deviation of the square droplet radius fluctuations, σ_{R^2}, increases in time as $t^{1/2}$; the growth rate depends linearly on the turbulent scale separation parametrized by Re_λ. As shown in Fig. 2, for a cloud with $\mathrm{Re}_\lambda = 10000$—a typical value estimated in cumuli with integral scale of 100 m [8]—our expression predicts that σ_{R^2} reaches values in line with observations in real clouds (see [15], their Fig. 4) on time scales of less than 20 min.

The stochastic approach proposed here may be generalized to consider additional physics and adapted to different microscale phenomena in turbulent environments; this may also require a numerical solution of the governing Langevin equations, something still order of magnitudes cheaper than a fully-resolved DNS. Indeed our analytical relation predicts numerical results requiring 10^{17} degrees of freedom. From a practical viewpoint, this indicates the promising potential of modeling approaches based on PDFs.

Our results represent a lower limit for the impact of turbulence on warm rain formation since real clouds typically exceed 100 m in scale and are in general nonhomogeneous, featuring a fluctuating temperature field and vigorous entrainment of relatively dry air from outside the cloud leading to enhanced supersaturation fluctuations within the cloud. These additional effects would lead to even larger values of σ_{R^2}, more than sufficient to explain the spectral broadening observed in real clouds.

This work was supported by the Swedish e-Science Research Centre SeRC, and by the European Research Council Grant No. ERC-2013-CoG-616186, TRITOS. Computer time provided by SNIC (Swedish National Infrastructure for Computing) is gratefully acknowledged.

*gaetano.sardina@misu.su.se

[1] J. R. Taylor and R. Stocker, Science **338**, 675 (2012).
[2] A. Johansen, J. S. Oishi, M.-M. Mac Low, H. Klahr, T. Henning, and A. Youdin, Nature (London) **448**, 1022 (2007).
[3] P. Jenny, D. Roekaerts, and N. Beishuizen, Prog. Energy Combust. Sci. **38**, 846 (2012).
[4] J. Bec, H. Homann, and G. Krstulovic, Phys. Rev. Lett. **112**, 234503 (2014).
[5] H. Shiogama and T. Ogura, Nature (London) **505**, 34 (2014).
[6] R. A. Shaw, Annu. Rev. Fluid Mech. **35**, 183 (2003).
[7] E. Bodenschatz, S. P. Malinowski, R. A. Shaw, and F. Stratmann, Science **327**, 970 (2010).
[8] W. W. Grabowski and L.-P. Wang, Annu. Rev. Fluid Mech. **45**, 293 (2013).
[9] S. Sundaram and L. R. Collins, J. Fluid Mech. **335**, 75 (1997).
[10] J. Bec, H. Homann, and S. S. Ray, Phys. Rev. Lett. **112**, 184501 (2014).
[11] G. Falkovich, A. Fouxon, and M. Stepanov, Nature (London) **419**, 151 (2002).
[12] W. A. Cooper, J. Atmos. Sci. **46**, 1301 (1989).
[13] M. Kulmala, Ü. Rannik, E. L. Zapadinsky, and C. F. Clement, J. Aerosol Sci. **28**, 1395 (1997).
[14] P. Vaillancourt, M. Yau, and W. Grabowski, J. Atmos. Sci. **58**, 1945 (2001).
[15] J.-L. Brenguier and L. Chaumat, J. Atmos. Sci. **58**, 628 (2001).
[16] A. Celani, A. Mazzino, A. Seminara, and M. Tizzi, J. Turbul. **8**, N17 (2007).
[17] A. Celani, G. Falkovich, A. Mazzino, and A. Seminara, Europhys. Lett. **70**, 775 (2005).
[18] R. Paoli and K. Shariff, J. Atmos. Sci. **66**, 723 (2009).
[19] A. S. Lanotte, A. Seminara, and F. Toschi, J. Atmos. Sci. **66**, 1685 (2009).
[20] See Supplemental Material at http://link.aps.org/supplemental/10.1103/PhysRevLett.115.184501, which includes Refs. [21–26], for details on the physical models, further information on the numerical scheme, and additional results.
[21] H. Siebert, K. Lehmann, and M. Wendisch, J. Atmos. Sci. **63**, 1451 (2006).
[22] B. Kumar, J. Schumacher, and R. A. Shaw, Theor. Comput. Fluid Dyn. **27**, 361 (2013).
[23] P. A. Vaillancourt and M. K. Yau, Bull. Am. Meteorol. Soc. **81**, 285 (2000).
[24] R. Rogallo, Numerical experiments in homogeneous turbulence, NASA Technical Report No. 81835, 1981.
[25] V. Eswaran and S. Pope, Comput. Fluids **16**, 257 (1988).
[26] J. Smagorinsky, Mon. Weather Rev. **91**, 99 (1963).
[27] S. Twomey, Pure Appl. Geophys. **43**, 243 (1959).
[28] H. Pruppacher and J. Klett, *Microphysics of Clouds and Precipitation* (Kluwer Academic, Dordrecht, 1997).
[29] S. B. Pope, *Turbulent Flows* (Cambridge University Press, Cambridge, England, 2000).
[30] B. Kumar, J. Schumacher, and R. A. Shaw, J. Atmos. Sci. **71**, 2564 (2014).
[31] C. Zhan, G. Sardina, E. Lushi, and L. Brandt, J. Fluid Mech. **739**, 22 (2014).
[32] F. Ditas, R. Shaw, H. Siebert, M. Simmel, B. Wehner, and A. Wiedensohler, Atmos. Chem. Phys. **12**, 2459 (2012).

Supplemental material for "Continuous growth of droplet size variance due to condensation in turbulent cloud"

Gaetano Sardina,[1,*] Francesco Picano,[2,3] Luca Brandt,[2] and Rodrigo Caballero[1]

[1]*Department of Meteorology and SeRC, Stockholm University, Stockholm, Sweden*
[2]*Linné FLOW Centre and SeRC, KTH Mechanics, Stockholm, Sweden*
[3]*Department of Industrial Engineering, University of Padova, Padova, Italy*

(Dated: October 8, 2015)

SECTION A. EULERIAN-LAGRANGIAN PHYSICAL CLOUD MODEL

Derivation of the supersaturation equation

The equation governing the evolution of the supersaturation can be derived from first principles, vapor mass and energy conservation, and thermodynamics relations. Since the supersaturation is a thermodynamic variable (as temperature, internal energy and entropy) one can write a conservation equation. The original derivation by Twomey that can be found in textbooks of atmospheric physics is obtained neglecting the effects of viscosity [1, 2], which we include below in the most general case.

The supersaturation s is defined as $s = q_v/q_{vs} - 1$ where q_v is the vapor mixing ratio and q_{vs} its saturated value. The supersaturation rate of change is obtained by differentiating its definition:

$$\frac{Ds}{Dt} = \frac{1}{q_{vs}}\frac{Dq_v}{Dt} - \frac{q_v}{q_{vs}^2}\frac{Dq_{vs}}{Dt} \tag{1}$$

The vapor mixing ratio follows the conservation equation:

$$\frac{Dq_v}{Dt} = D_v\nabla^2 q_v - C_d \tag{2}$$

where D_v is the thermal diffusivity of water vapor in air and C_d is the condensation rate. An evolution equation for q_{vs} is obtained from the Clasius-Clapeyron equation linking supersaturation pressure e_s with temperature θ:

$$\frac{Dq_{vs}}{Dt} = \frac{D}{Dt}\left(\frac{\epsilon e_s}{p}\right) = \frac{\epsilon}{p}\frac{De_s}{Dt} - \frac{\epsilon e_s}{p^2}\frac{Dp}{Dt} = \\ = \frac{\epsilon}{p}\frac{de_s}{d\theta}\frac{D\theta}{Dt} - \frac{\epsilon e_s}{p^2}\frac{Dp}{Dt} = \frac{\epsilon L e_s}{pR_v\theta^2}\frac{D\theta}{Dt} - \frac{\epsilon e_s}{p^2}\frac{Dp}{Dt} \tag{3}$$

where ϵ is the ratio between water and dry air molecular weights, p is the thermodynamic pressure, R_v is the gas costant for water vapor and L is the latent heat of evaporation. The temperature θ obeys energy conservation:

$$\frac{D\theta}{Dt} = \kappa_\theta\nabla^2\theta - \frac{g}{c_p}w + \frac{L}{c_p}C_d \tag{4}$$

where k_θ is the thermal diffusivity, g the gravity acceleration, c_p is the specific heat at costant pressure and w the vertical fluid velocity component. The pressure p can be obtained from hydrostatic equilibrium:

$$\frac{Dp}{Dt} = -\frac{gp}{R_a\theta}w \tag{5}$$

where R_a is the gas costant for dry air. Substituting Eqs. (5) and (4) in Eq. (3) results in:

$$\frac{Dq_{vs}}{Dt} = \left(\frac{\epsilon e_s g}{pR_a\theta} - \frac{\epsilon e_s g L}{pR_v\theta^2 c_p}\right)w + \frac{\epsilon e_s k_\theta L}{pR_v\theta^2}\nabla^2\theta + \frac{\epsilon e_s L^2}{pR_v\theta^2 c_p}C_d \tag{6}$$

and consequently Eq. (1) becomes:

$$\frac{Ds}{Dt} = \frac{1}{q_{vs}}D_v\nabla^2 q_v - \frac{C_d}{q_{vs}} + \frac{s+1}{q_{vs}}\left(\frac{\epsilon e_s g L}{pR_v\theta^2 c_p} - \frac{\epsilon e_s g}{pR_a\theta}\right)w + \\ - \frac{s+1}{q_{vs}}\frac{\epsilon e_s k_\theta L}{pR_v\theta^2}\nabla^2\theta - \frac{s+1}{q_{vs}}\frac{\epsilon e_s L^2}{pR_v\theta^2 c_p}C_d. \tag{7}$$

Assuming $s \ll 1$ and substituting the expression of q_{vs}, the previous equation reads:

$$\frac{Ds}{Dt} = \left(\frac{gL}{R_v\theta^2 c_p} - \frac{g}{R_a\theta}\right)w - \left(\frac{p}{\epsilon e_s} + \frac{L^2}{R_v c_p\theta^2}\right)C_d \\ + \frac{pD_v}{\epsilon e_s}\nabla^2 q_v - \frac{k_\theta L}{R_v\theta^2}\nabla^2\theta, \tag{8}$$

where we defined

$$A_1(\theta) = \frac{gL}{R_v c_p\theta^2} - \frac{g}{R_a\theta} \tag{9}$$

$$A_2(\theta) = \frac{R_a\theta}{\epsilon e_s(\theta)} + \frac{\epsilon L^2}{p\theta c_p} \tag{10}$$

$$A_3(\theta) = \left(\frac{\rho_w R_v\theta}{D_v e_s(\theta)} + \frac{\rho_w L^2}{k_\theta R_v\theta^2}\right)^{-1} \tag{11}$$

and

$$C_d = \frac{4\pi\rho_w A_3}{\rho V}s\sum R_i \tag{12}$$

The supersaturation relaxation time is

$$\tau_s(\theta) = \left(4\pi\rho_w A_2(\theta)A_3(\theta)\sum R_i/V\right)^{-1} \tag{13}$$

where ρ_w is the water density and R_i are the radii of the droplets in the volume V. Eq. (8) can be exactly re-written as

$$\frac{Ds}{Dt} = A_1 w - \frac{s}{\tau_s} + \frac{pD_v}{\epsilon e_s}\nabla^2 q_v - \frac{k_\theta L}{R_v\theta^2}\nabla^2\theta. \tag{14}$$

The only assumption in the model is introduced now, assuming the diffusive terms proportional to the laplacian of the supersaturation

$$k\nabla^2 s = \frac{pD_v}{\epsilon e_s}\nabla^2 q_v - \frac{k_\theta L}{R_v\theta^2}\nabla^2\theta \tag{15}$$

obtaining the final equation for the supersaturation field

$$\frac{Ds}{Dt} = A_1 w - \frac{s}{\tau_s} + k\nabla^2 s. \tag{16}$$

Given the high Reynolds numbers inside clouds it appears reasonable to assume that diffusion and viscous effects are much smaller than the convective transport. Indeed, we will show in Section B that the diffusive term does not affect the supersaturation for large cloud dimensions. The term $A_1 w$ is a source/sink term of supersaturation resulting from the variation in temperature and pressure with height.

Model equations and parameters

The complete Eulerian set of equations for the turbulent velocity field $\mathbf{u}$, the supersaturation s, the temperature fluctuations θ, the vapor mixing ratio q_v and the buoyancy B therefore reads

$$\nabla\cdot\mathbf{u} = 0, \tag{17}$$

$$\frac{\partial\mathbf{u}}{\partial t} + \mathbf{u}\cdot\nabla\mathbf{u} = -\frac{\nabla p'}{\rho} + \nu\nabla^2\mathbf{u} + B\mathbf{e_z} + \mathbf{f}, \tag{18}$$

$$\frac{\partial s}{\partial t} + \mathbf{u}\cdot\nabla s = \kappa\nabla^2 s + A_1(\theta)w - \frac{s}{\tau_s(\theta)}, \tag{19}$$

$$\frac{\partial\theta}{\partial t} + \mathbf{u}\cdot\nabla\theta = \kappa_\theta\nabla^2\theta - \frac{g}{c_p}w + \frac{L}{c_p}C_d, \tag{20}$$

$$q_v = q_{vs}(\theta)(s+1), \tag{21}$$

$$B = g\left[\frac{\theta-\theta_0}{\theta_0} + \epsilon(q_v - q_{v0}) - q_w\right]. \tag{22}$$

The velocity field $\mathbf{u}$ obeys the Navier-Stokes-Boussinesq equations, (18), where p' is the pressure deviation from its hydrostatic value, ρ is the density of air, $\mathbf{f}$ an external forcing acting just at the larger turbulent scales, ν the kinematic viscosity. The external forcing $\mathbf{f}$ maintains a turbulent field in the steady state regime.

In the most general cases turbulent clouds are a transient phenomenon. The transient effects are relevant when observing the cloud for its whole life-time, especially during the cloud generation and dissipation phase. The total life-time of a cloud is of the order of hours/days; however, if we study droplet condensation for time intervals of the order of minutes, we can consider the system at quasi statistical steady-state, as shown by experimental observations in real clouds as shallow cumulus clouds [3] and marine stratocumulus clouds [4]. Most of the DNS of clouds available in literature assume steady state turbulence [5–9]. The temperature follows the advection-diffusion equation (20). Equation (21) links the vapor mixing ratio q_v, with its saturated value $q_{vs} = q_{vs}(\theta, s)$ function of the temperature and the supersaturation field. The momentum equation is forced by the buoyancy field B, expressed by equation (22), where θ_0 is the reference temperature, q_{v0} is the vapor mixing ratio at θ_0 and $s = 0$, q_w is the water mixing ratio and represents the droplet drag on the flow. In adiabatic cloud cores, the buoyancy effects are assumed to be negligible [10].

The Eulerian fields are coupled with the Lagrangian equation for the droplet evolution:

$$\frac{d\mathbf{v_d}}{dt} = \frac{\mathbf{u}(\mathbf{x_d}, t) - \mathbf{v_d}}{\tau_d} - g\mathbf{e_z}, \tag{23}$$

$$\frac{d\mathbf{x_d}}{dt} = \mathbf{v_d}, \tag{24}$$

$$\frac{dR_i^2}{dt} = 2A_3(\theta)s(\mathbf{x_d}, t) \tag{25}$$

with $\mathbf{x_d}$ and $\mathbf{v_d}$ the droplet position and velocity, $\mathbf{u}(\mathbf{x_d}, t)$ and $s(\mathbf{x_d}, t)$ the fluid velocity and supersaturation field at droplet position, $\tau_d = 2\rho_w R_i^2/(9\rho\nu)$ the droplet relaxation time. The droplets are assumed to be spherical, with radius smaller than the Kolmogorov scale in order to be considered point-particles. The only forces acting on the droplets are the Stokes drag and the gravitational force.

Computational methodology

The numerical data set described in the manuscript has been obtained from Direct Numerical Simulations (DNS) using a classical pseudo-spectral method for the Eulerian equations coupled with a Lagrangian solver for the droplets. For the fluid phase, the Navier–Stokes–Boussinesq equations have been integrated in a three-periodic domain using a Fourier spectral method with the nonlinear terms de-aliased by the 3/2 rule. The solution is advanced in time using a third-order low-storage Runge–Kutta method; specifically, the nonlinear terms are computed using an Adam–Bashforth-like approximation while the diffusive terms are analytically integrated [11]. The random forcing $\mathbf{f}$ is applied isotropically to the first shell of wave vectors, with fixed amplitude, constant in time and uniformly distributed in phase and directions [12]. For the dispersed phase, we use the point-particle approximation as typical droplet sizes are smaller than the flow Kolmogorov length. The same Runge–Kutta temporal integration used for the carrier phase is adopted for the Lagrangian equations. A trilinear interpolation scheme is used to compute the flow velocity, supersaturation and temperature at the particle position. The correspondent trilinear extrapolation scheme is adopted to

transfer the information from the droplet location (supersaturation, radius, temperature) into the Eulerian grid. The code is fully MPI parallelized to be efficiently run on supercomputing infrastructures with a performance linearly scaling up to 10^4 cores.

SECTION B. NUMERICAL MODELS

Constant coefficient model

The system of differential and algebraic equations (1-14) can be simplified assuming that the coefficients A_1, A_2, A_3 are only function of the reference temperature θ_0, i.e. the temperature fluctuations can be neglected for their calculation [7, 9], and the buoyancy term can be neglected as well [10]. To check and quantify the order of magnitude of the temperature fluctuations, we performed a preliminary DNS simulation solving the complete system (1-14). The simulation matches the parameters described in case DNS $D1$ of the manuscript. In particular, we simulate a cloud of length $L_{box} = 1.5$ m, velocity fluctuations $v_{rms} = 0.1$ m/s, Taylor Reynolds number $Re_\lambda = 390$ with a resolution of 1024^3 grid points and 4.4×10^8 Lagrangian droplets. From the numerical results we obtain a negligible value of the temperature root mean square $\theta_{rms} = 5 \times 10^{-3}$ K. Since, the supersaturation depends on a non-trivial way on the turbulent field via the quantities A_2, A_3, τ_s and the Clasius-Clapeyron equation, it is relevant to examine the behavior of its probability distribution function (pdf). Figure 1 shows the pdf of the supersaturations fluctuations for the full set of equations (DNS): the behavior is Gaussian and equal to the two results from the constant coefficient model reported in the manuscript.

Direct Numerical Simulation (DNS) of the reduced model

As seen in the previous paragraph, we can assume that the temperature field is constant in time and space and equals to its reference value θ_0 for the calculation of the constants A_1, A_2 and A_3 while the fluctuations still affect the evaporation-condensation via the supersaturation equation. This has two consequences: the physics of the system is simpler to investigate and the numerical solver is faster since the equations are more easy to manage. Under the simplifying hypothesis the system (1-14) reduces to:

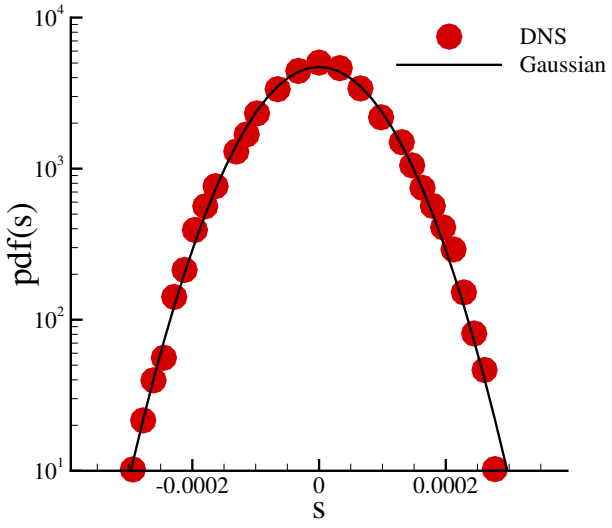

FIG. 1: Probability distribution function of the supersaturation fluctuations extracted by the DNS simulation (symbols) and comparison with its Gaussian fit (line).

$$\nabla \cdot \mathbf{u} = 0, \tag{26}$$

$$\frac{\partial \mathbf{u}}{\partial t} + \mathbf{u} \cdot \nabla \mathbf{u} = -\frac{\nabla p'}{\rho} + \nu \nabla^2 \mathbf{u} + \mathbf{f}, \tag{27}$$

$$\frac{\partial s}{\partial t} + \mathbf{u} \cdot \nabla s = \kappa \nabla^2 s + A_1 w - \frac{s}{\tau_s}, \tag{28}$$

$$\frac{d\mathbf{v_d}}{dt} = \frac{\mathbf{u}(\mathbf{x_d}, t) - \mathbf{v_d}}{\tau_d} - g\mathbf{e_z}, \tag{29}$$

$$\frac{d\mathbf{x_d}}{dt} = \mathbf{v_d}, \tag{30}$$

$$\frac{dR_i^2}{dt} = 2A_3 s(\mathbf{x_d}, t) \tag{31}$$

where A_1, A_2 and A_3 are constant that depends on the reference temperature θ_0. The system (15-20) can be numerically solved without any further hypothesis, simplifications or models via Direct Numerical Simulations. In the manuscript we performed 8 different DNS cases described, see Table I, the largest corresponding to a cloud of the order of $L_{box} = 3$ m (DNS E1) with a resolution of 10^{10} degrees of freedom including the Eulerian grid points (2048^3) and Lagrangian droplets (3×10^9).

Large Eddy Simulation (LES)

Since the largest DNS simulation allows us to describe core clouds of the order of 3 meters, we need to employ Large Eddy Simulations (LES) to study clouds with size of about 100 meters. The LES equations are obtained from the DNS system by applying a low-pass filter to the

Eulerian fields that remove the smallest scales. In this way, just the large scales are evolved while the effects of the small scales on the large ones is modeled. The generic Eulerian field f can be decomposed in a filtered or resolved component $\bar{f}$ and a residual or subgrid-scale component f_{sgs}. Applying the filter operator to the system (15-20), we obtain:

$$\nabla \cdot \bar{\mathbf{u}} = 0, \tag{32}$$

$$\frac{\partial \bar{\mathbf{u}}}{\partial t} + \bar{\mathbf{u}} \cdot \nabla \bar{\mathbf{u}} = -\frac{\nabla \bar{p}}{\rho} + \nu \nabla^2 \bar{\mathbf{u}} + \bar{\mathbf{f}} + \nabla \cdot \bar{\tau}_{sgs}, \tag{33}$$

$$\frac{\partial \bar{s}}{\partial t} + \bar{\mathbf{u}} \cdot \nabla \bar{s} = \kappa \nabla^2 \bar{s} + A_1 \bar{w} - \frac{\bar{s}}{\tau_s} + \nabla \cdot \bar{\mathbf{J}}_{sgs}, \tag{34}$$

$$\frac{d\mathbf{v_d}}{dt} = \frac{\bar{\mathbf{u}}(\mathbf{x_d}, t) + \mathbf{u_{sgs}}(\mathbf{x_d}, t) - \mathbf{v_d}}{\tau_d} - g\mathbf{e_z}, \tag{35}$$

$$\frac{d\mathbf{x_d}}{dt} = \mathbf{v_d}, \tag{36}$$

$$\frac{dR_i^2}{dt} = 2A_3 \left(\bar{s}(\mathbf{x_d}, t) + s_{sgs}(\mathbf{x_d}, t)\right) \tag{37}$$

where $\bar{\tau}_{sgs}$, $\bar{\mathbf{J}}_{sgs}$, $\mathbf{u_{sgs}}$ and s_{sgs} are respectively the subgrid stress tensor, the subgrid supersaturation flux, the subgrid velocity and the subgrid supersaturation. The subgrid terms should be described using suitable closure models, which introduce an unavoidable approximation of the physics with respect to the DNS. Here, the subgrid stress tensor $\bar{\tau}_{sgs}$ and the subgrid supersaturation flux $\bar{\mathbf{J}}_{sgs}$ are modelled with to the classic Smagorinski closure [13]. The subgrid terms appearing in the Lagrangian droplet equation $\mathbf{u_{sgs}}$ and s_{sgs} are set to zero so to consider our LES results as a lower limit for the droplet size distribution in the cloud. Infact, considering the temporal evolution of the droplet square radius fluctuations:

$$\frac{d\langle (R_i^{2'})^2 \rangle}{dt} = \frac{d\sigma_{R^2}^2}{dt} = 4A_3 \left(\langle \bar{s}' R^{2'} \rangle + \langle s'_{sgs} R^{2'} \rangle \right) \tag{38}$$

we are implicitly assuming that the subgrid correlations $\langle s'_{sgs} R^{2'} \rangle$ are much smaller than the resolved scale correlations $\langle \bar{s}' R^{2'} \rangle$. This is justified by the DNS results represented in the inset of figure 1 of the main manuscript where the correlation $\langle s' R^{2'} \rangle$ is displayed. The figure shows that the large DNS gives values of this correlation two order of magnitude larger than that from the smaller simulations.

Another approximation introduced in the LES is related to the number of droplets tracked in the simulation. Theoretically, one should evolve order 10^{14} droplets which is unfeasible. We therefore use the method of droplet renormalization described in [7]. We validated the LES by comparing the results with our finest DNS simulation, DNS E1. Different LES simulations have been performed with different resolutions down to 32^3 grid points. The root mean square of the square droplet radius fluctuations (top panel) and of the supersaturation fluctuations (bottom panel) are shown in figure 2 for the DNS and LES. The LES slightly underestimates the observable $\sigma_{R^2}^2$ and s_{rms} as expected from equation (38). The agreement between LES and DNS is excellent considering that we used 10^5 degrees of freedom against 10^{10} for the DNS. This implies that just solving the larger scales is enough to provide a good prediction of the droplet size spectra variance. In conclusion, the LES simulation is able to give a lower limit of the droplet spectra broadening at a moderate computational cost.

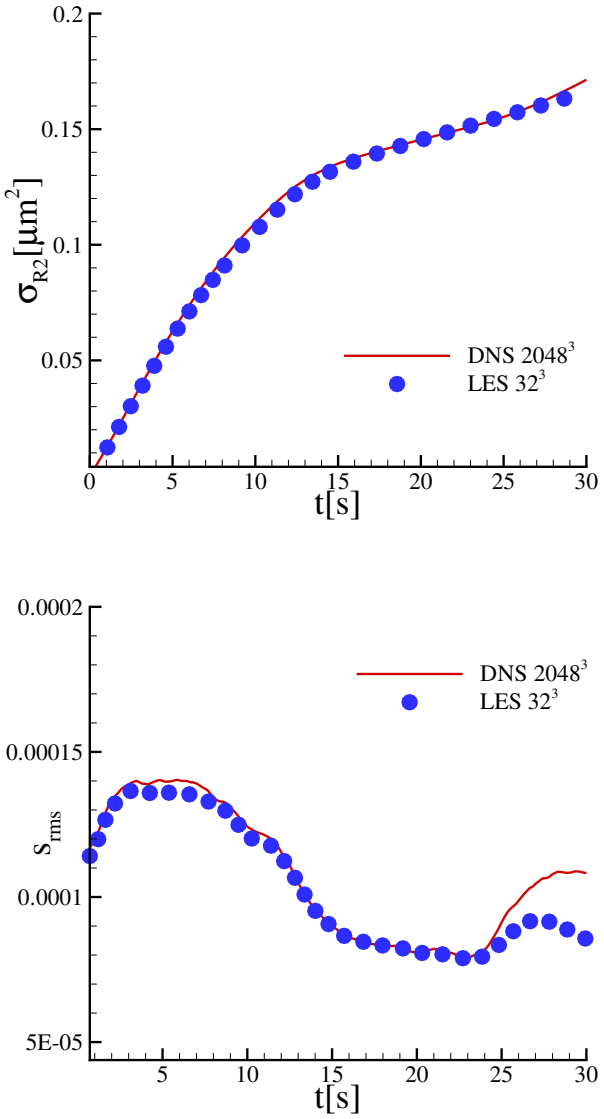

FIG. 2: Top panel: comparison between the root mean square of the square droplet radius fluctuations σ_{R^2} versus time for the LES (symbols) and the DNS simulations. Bottom panel: comparison between the root mean square of the supersaturation fluctuations versus time for the LES (symbols) and the DNS simulations.

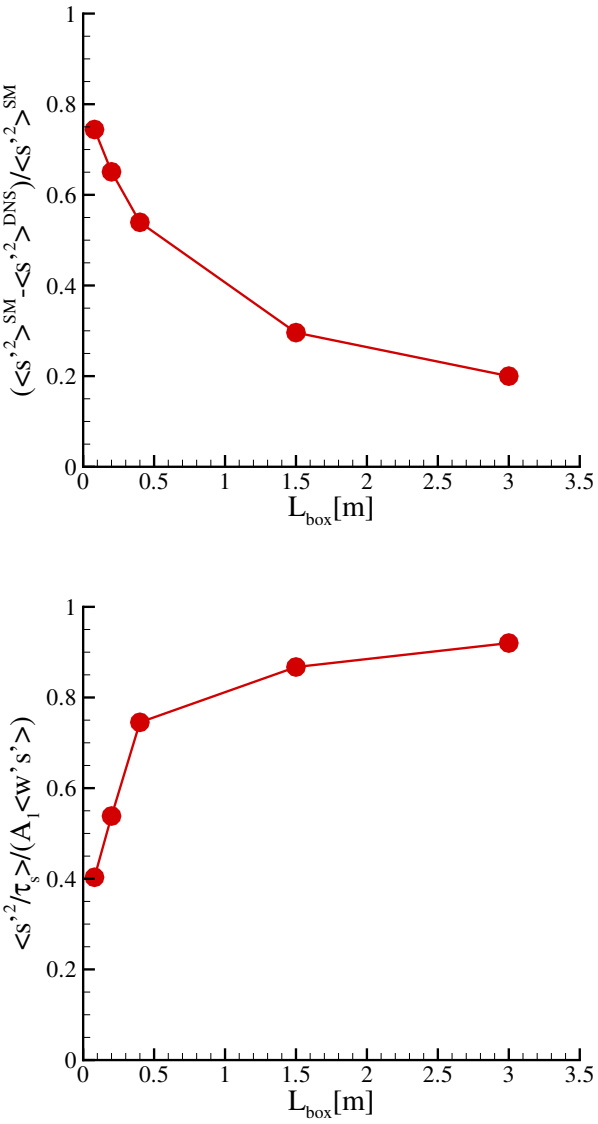

FIG. 3: Top panel: Relative error pertaining the quasi steady-state supersaturation fluctuation variance in the stochastic model (SM) and DNS. Bottom panel: ratio between the droplet sink term and the source term in the supersaturation variance equation (28).

Stochastic model (SM)

The other approach we used in our work is the stochastic model described by the equations (6-7) in the main manuscript. We show in the main text that the stochastic model tends to overestimate the droplet-related quantities and that the differences become smaller by increasing the ratio between the large and the small scales in the numerical simulations. A systematic study of the difference between the stochastic model and the DNS is presented in this section.

The relative error pertaining the quasi steady-state value of the supersaturation fluctuation variance is reported in the top panel of figure 3 versus the cloud size domain (the size of the computational domain and the large-to-small scale ratio). A large error is evident for clouds of smaller size and the differences are monotonically decreasing when increasing the large-to-small scale ratio (i.e. the Reynolds number). For clouds that are of the order of 100 meters, our prediction has a margin of error lower than 20 %, an acceptable value for statistical observables that DNS cannot calculate with the current computational resources.

The error in the stochastic model can be explained by viscous effects in the supersaturation fluctuations. Multiplying equation (17) with the supersaturation fluctuations and averaging, we obtain an equation for the supersaturation variance:

$$\frac{\partial \langle s'^2/2\rangle}{\partial t} + \nabla \cdot \langle \mathbf{u}' s'^2/2\rangle = -\kappa \langle (\nabla s')^2\rangle + A_1 \langle w' s'\rangle - \langle \frac{s'^2}{\tau_s}\rangle \tag{39}$$

where the left hand side is zero at statistically steady state, and a balance between three terms holds: viscous dissipation $\kappa\langle(\nabla s')^2\rangle$, production $A_1\langle w's'\rangle$ and droplet sink $\langle s'^2/\tau_s\rangle$. In the case of the classic inviscid Twomey equation (employed also in the stochastic model) the balance is only between production and the droplet sink terms, and viscous effects are neglected. To quantify the differences between the inviscid and viscid Twomey equation, we display the ratio between the droplet sink and the production term as extracted from the DNS in the bottom panel of figure 3, where a value of this ratio equal to 1 corresponds to an inviscid behavior as assumed in the Towmey model. For smaller clouds, the ratio is about 0.5 so that just half of the supersaturation fluctuations induce the droplet growth while the remaining is diffused. This explain why the stochastic model, neglecting diffusion, is not able to predict the DNS results. By increasing the Reynolds number and the size of the cloud, the ratio $\langle s'^2/\tau_s\rangle / A_1\langle w's'\rangle$ tends to 1, meaning that the viscous effects become more and more negligible (they vanish in the limit of infinite Reynolds number). Therefore, the stochastic model effectively predicts an upper limit for the droplet spectral broadening at a zero computational cost. In conclusion, the DNS results will always lie between the LES estimation (lower limit) and the stochastic model prediction (upper limit).

* gaetano.sardina@misu.su.se

[1] S. Twomey, Pure Appl. Geophys. **43**, 243 (1959).
[2] H. Pruppacher and J. Klett, *Microphysics of clouds and precipitation* (1997).
[3] H. Siebert, K. Lehmann, and M. Wendisch, J. Atmos. Sci. **63**, 1451 (2006).

[4] F. Ditas, R. Shaw, H. Siebert, M. Simmel, B. Wehner, and A. Wiedensohler, Atmos. Chem. Phys. **12**, 2459 (2012).
[5] P. Vaillancourt, M. Yau, and W. Grabowski, J. Atmos. Sci. **58**, 1945 (2001).
[6] R. Paoli and K. Shariff, J. Atmos. Sci. **66** (2009).
[7] A. S. Lanotte, A. Seminara, and F. Toschi, J. Atmos. Sci. **66** (2009).
[8] B. Kumar, J. Schumacher, and R. A. Shaw, J. Atmos. Sci. **71**, 25642580 (2014).
[9] B. Kumar, J. Schumacher, and R. A. Shaw, Theor. Comp. Fluid Dyn. **27**, 361 (2013).
[10] P. A. Vaillancourt and M. Yau, B. Am. Metereolog. Soc. **81**, 285 (2000).
[11] R. Rogallo, NASA STI/Recon Technical Report N **81**, 31508 (1981).
[12] V. Eswaran and S. Pope, Comput. Fluids **16**, 257 (1988).
[13] J. Smagorinsky, Mon. Weather Rev. **91**, 99 (1963).